Groundwater Flow Monitoring via Joint Time-lapse Electrical Resistivity and Self Potential Data Tomography

Lige Bai[1], jing li[1], Jiawei Tan[1], Hui Liu[1], and Tianqi Wang[1]

[1]Jilin University

April 28, 2020

Abstract

Revealing the dynamics of groundwater movement in the vadose zone is crucial to groundwater management and artificial recharge. In this study, the groundwater flow characterization of the pumping process is monitored by the joint time-lapse electrical resistivity tomography (ERT) and self-potential (SP) data tomography. The ERT data invert the resistivity distribution, which relates to the variation of soil moisture content during the pumping process. Base on the groundwater motion feature, the SP data provide a direct way to invert the current density and estimate the permeability. A total of 24 hours of time-lapse surveys show a significant increase and decrease in resistivity and permeability during water pumping and groundwater recharge, which suggests groundwater decline and recovery process. These results have an excellent agreement with the groundwater level monitoring result. Combining ERT and SP data can provide a reliable way in groundwater or other hydrogeological surveys.

Groundwater Flow Monitoring via Joint Time-lapse Electrical Resistivity and Self Potential Data Tomography

Lige Bai[1], Jing Li[1*], Hui Liu[1], Jaiwei Tan[1], Tianqi Wang[1]

[1] College of geo-exploration Sci. &Tech, Jilin University, Changchun, Jilin 130026, China

*Corresponding author: Jing Li,*inter.lijing@gmail.com*

Key words: Groundwater Flow Monitoring; Time-lapse; Electrical Resistivity Tomography (ERT); Self-potential (SP) Tomography

Funding Information: This work are supported by the Natural Science Foundation of China (41874134), the Jilin Excellent Youth Fund (20190103142JH) and the China Postdoctoral Science Foundation 2015M571366

Summary

Revealing the dynamics of groundwater movement in the vadose zone is crucial to groundwater management and artificial recharge. In this study, the groundwater flow characterization of the pumping process is monitored by the joint time-lapse electrical resistivity tomography (ERT) and self-potential (SP) data tomography. The ERT data invert the resistivity distribution, which relates to the variation of soil moisture content during the pumping process. Base on the groundwater motion feature, the SP data provide a direct way to invert the current density and estimate the permeability. A total of 24 hours of time-lapse surveys show a significant increase and decrease in resistivity and permeability during water pumping and groundwater recharge, which suggests groundwater decline and recovery process. These results have an excellent agreement with the groundwater level monitoring result. Combining ERT and SP data can provide a reliable way in groundwater or other hydrogeological surveys.

1 Introduction

The groundwater flow or level variation is crucial to groundwater management and site soil pollution control (Tesfaldet et al., 2019). To understand the location and timing of groundwater traveling through the vadose zone, we must investigate groundwater flow characterization and recharge mechanism. The traditional hydrographic groundwater surveys usually include float observation, pressure observation, and automatic tracking observation. However, when measuring the dynamic change of groundwater level or content over a long period, the measurement is usually indirect, difficult, costly, and infrequent, except for the traditional methods such as volume weighing and borehole sampling to detect the properties of groundwater (Ogilvy et al., 2009). In contrast, the nonintrusive time-lapse geophysics tools provide an opportunity to complement hydraulic campaigns (Fetter, 2001) since they can be implemented over a large region with dense sampling in both space and time. In particular, electrical resistivity tomography (ERT) and self-potential (SP) tomography are particularly appropriate to monitoring groundwater dynamics in resistivity and apparent current density because it is sensitive to changes in flow or chemistry (Carey, 2017; Revil & Linde, 2006). The time-lapse method carries out periodic measurements at a fixed location and provides the perception of the 2D/3D groundwater flow by analyzing the response variation in the subsurface. Compared with the hydrographic survey, and it is a non-invasive, practical, and cost-effective method for characterizing and delineating special recharge zones.

The time-lapse ERT is a mature technology for the hydrogeological study. There have been many recent examples of applying this technology for vadose zone soil moisture estimation, groundwater flow monitoring based on the resistivity characteristic (Jongmans & Garambois, 2007; Niesner, 2010). It measures the resistivity of the subsurface by using an electrode dipole to inject direct current into the ground and using additional dipoles to measure the resulting voltage. Many studies have explored the challenges and uncertainties associated with predicting groundwater flow using ERT. However, the ERT method is an indirect approach that depends on the change of soil moisture content. There are inherent uncertainties, and the sensitivity of ERT is also not enough for small-scale groundwater flow.

The SP method corresponds to the generation of an underground natural current source (Ahmed & Jardani, 2013). This method is used to monitor the groundwater based on the flow characteristic. Sill (1983) uses physical approaches to simulate the SP anomalies related to groundwater flow by solving major mathematical problems corresponding to groundwater flow problems. By observing the SP data on the ground surface, the potential distribution and current density distribution of the underground space can be effectively calculated to quantify the abnormal distribution characteristics. In recent years, the application of the natural potential method in the inversion of geophysical parameters, such as changes in the hydraulic head using SP technology to reconstruct pumping tests, has gradually attracted attention.

The ERT and SP method monitors the groundwater flow from different aspects. ERT utilizes the change of resistivity caused by the variations of moisture content in the soil. The groundwater movement produces the SP signal. These two methods have different physical mechanisms to describe groundwater flow characterization. Therefore, it is necessary to use a variety of geophysics methods for cross-validation and interpretation using ground truth constraints. This study addressed two primary questions: 1) What is the advantage of the joint time-lapse strategy; and 2) How does the magnitude and timing of water input change groundwater flow dynamics? To answer these questions, we propose the joint ERT and SP method strategy to monitor the groundwater flow variation in the pumping experiment. The groundwater level is controlled by pumping water from well to create various conditions of groundwater flow. The ERT data invert the resistivity distribution, which relates to the soil moisture content. Then, we combine the SP data and resistivity result to invert the apparent current density and estimate the permeability.

The paper is organized as follows. After the introduction, we introduce the basic forward and inversion theory of SP data. By solving the hydraulic problem and the Poisson equation, the underground current density distribution is restored. Then, the pumping experiment is used to test the ability of ERT and SP data in groundwater flow monitoring. The final sections are the conclusion and discussions.

2 The Self-potential Inversion Theory

Self-potential (SP) refers to passively measure electric potentials that are generated through coupling with some other forcing mechanism, which is often hydraulic, chemical, or thermal. This coupled flow mechanism in this stratigraphic setting was detected on the surface by Minsley, (2007). Over the years, there has been a growing interest in the application of the SP method in various fields of earth science, including hydrology, geothermal and geotechnical and environmental engineering (Darnet& Marquis, 2004). In many cases, this method is relatively easy to use and convenient for qualitative interpretation. In this section, the forward and inverse problems of the SP method will be introduced. Meanwhile, the permeability tensor can be determined directly according to the coupling coefficient. The problem can then be determined independently by resistivity tomography.

2.1 Forward Modeling

Use the constitutive equation to explain the hydraulic problems of heterogeneous and anisotropic porous materials:

$$\left\{\begin{array}{r} a\frac{\partial h}{\partial t} + \nabla \bullet \mathbf{u} = Q_{\mathbf{s}} \\ \mathbf{u} = -K\nabla h \end{array}\right. \quad (2.1)$$

Where h denotes the hydraulic head (in m), a (m^{-1}) denotes the Storage ratio, Qs denotes the external sources, u denotes the Darcy velocity ($\mathrm{m}\bullet\mathrm{s}^{-1}$), and K ($\mathrm{m}\bullet\mathrm{s}^{-1}$) denotes the Penetration rate. The pressure of pore fluid p (in pa) can be expressed as the relationship between the mass density of pore water (in $\mathrm{kg/m}^3$), the acceleration of gravity g (in $\mathrm{m/s}^2$), and the hydraulic head h (in m) p=$\rho_{\mathbf{f}} g(h-z)$. z(in m) is the constant elevation above a given datum.Eq1 should follow the first type boundary (Dirichlet) condition and the second type boundary (Neumann) condition while following the initial term.

$$\textit{Boundary} \left\{\begin{array}{r} h = h_D \text{ at } \Gamma_D \\ -nK\nabla h = q_0 \text{ at } \Gamma_N \end{array}\right. \quad \textit{(2.2)}$$

$$\textit{Initial} \quad h = h_0 \textit{ at } t = 0 \textit{ (2.3)}$$

After solving hydraulic problems, it is essential to analyze electrical problems. The sum of conductive current density (Ohm's Law)$-\sigma\nabla\psi$ and the current source density$\mathbf{j}_s$is the total current density $\mathbf{j}$($\mathrm{A/m}^2$) (Ahmed &Jardani, 2013).

$$\mathbf{j} = -\sigma\nabla\psi + \mathbf{j}_s \quad (2.4)$$

$$\mathbf{j}_s = Q_V\mathbf{u} \ (2.5)$$

Where ψ (in V) denotes the electrical potential, $\sigma$is the electrical conductivity tensor. $Q_V$is the effective excess charge density tensor of the pore water per unit pore volume. $Q_V$can be predicted from the permeability tensor according to (Jardani et al., 2007):

$$\log_{10} Q_V = -9.2 - 0.82 \log_{10} K \ (2.6)$$

According to the continuity equation of charge$\nabla\mathbf{j} = 0$:

$$\nabla \bullet (\sigma\nabla\psi) = \nabla \bullet \mathbf{j}_s (2.7)$$

Where a Neumann boundary condition Γ_{NV} is applied to the upper interface (air-ground) and a Dirichlet boundary conditionΓ_{DV} is applied to other boundaries. It can ensure that the response of the underground potential is received on the ground surface and does not spread to the surrounding ground floor. The boundary problem indicates that the anomaly contains some information related to the hydraulic flow path (Revil et al., 2010).

2.2 Inverse Problem

Source inversion is an ill-posed, non-unique problem that can be solved by incorporating model regularization into the inverse problem. According to the SP inversion method proposed by Ahmed and Jardani (2013), the spatial distribution of potential anomalies caused by the underground current density vector is obtained. Use on a set of points M:

$\psi\left(N\right) = \int_{\Omega} G\left(N, M\right)\mathbf{j}_s\left(M\right)\mathrm{dV} \quad (2.8)$

Where $\mathbf{j}_s(M)$ is the current density source at a set of points M, $\psi(N)$ is the potential at a set of N electrodes, and$G\left(N, M\right)$ represents the measured natural potential data at point N and is currently at point M Kernel matrix. The calculation of the G (N, M) kernel function depends on the selection of several parameters: 1)the conductivity value of the medium; 2) the number of discrete elements M. The kernel matrix can be solved by using the finite element method (Trujillo-Barreto et al., 2004).

$\phi_d = \left\|W_d(G\omega - \psi^{\mathrm{obs}})\right\|_2^2(2.9)$

$\psi^{\mathrm{obs}} = [\psi_1^{\mathrm{obs}}, \psi_2^{\mathrm{obs}}, \psi_3^{\mathrm{obs}}, \ldots, \psi_N^{\mathrm{obs}}]^T(2.10)$

$W_d = diag[\frac{1}{\delta_1}, \frac{1}{\delta_2}, \ldots, \frac{1}{\delta_N}](2.11)$

Where $\|\|_2$ is the L2 norm, G represents the kernel matrix of N $\times$ 2M (corresponding to the self-potential measured at each site), and ω is the current density j_s related to the potential and the kernel matrix G. ψ^{obs} denotes a vector of N elements corresponding to a set of self-potential data,W_d is a N $\times$ N diagonal weighted square matrix, and $\delta_1$denotes the square of the deviation (Linde et al., 2007). Because the inversion leads to the ill-posedness of the solution, a regularization term, and a depth weighting function ϕ_m are added to the analysis process to reduce the problem of overfitting. Establish the global objective function term ϕ_T (Menke, 1984):

$\phi_T = \phi_d + \phi_m = \left\|W_d(G\omega - \psi^{\mathrm{obs}})\right\|_2^2 + \lambda^2\left\|W_m(\omega - \omega_0)\right\|_2^2(2.12)$

$W_m = LW_z = (z_0 + z)^{-\frac{\beta}{2}}$denotes a depth-weighted matrix of N $\times$ 2M (Li & Oldenburg, 1998),z_0 denotes the observation height of the model unit, and $L$is the smoothness based on the first derivative of ω, $\beta$is a constant term between 1 and 4. λ denotes the regularized constraint term 0 <λ <[?], and the objective function of the above formula is in the standard form:

$\phi_T = \left\|G\omega - \psi^{\mathrm{obs}}\right\|_2^2 + \lambda\left\|\omega - \omega_0\right\|_2^2(2.13)$

Where$G$,ω,ψ^{obs},$L_P$are matrices deduced by the Elédn's algorithm based on QR decomposition (Elédn, 1977). The solution to finding the minimum value of the objective function ϕ_T (Hansen, 1998):

$min(\left\|G\omega - \psi^{\mathrm{obs}}\right\|_2^2 + \lambda\left\|\omega - \omega_0\right\|_2^2)(2.14)$

$\hat{\omega}\left(\lambda\right) = [G^T G + \lambda E]^{-1}(G^T\psi^{\mathrm{obs}} + \lambda\omega_0)(2.15)$

When the permeability is known, the current density distribution can be calculated for the prior model of the objective function, and in the case where there is no prior model$\omega_0 = 0$:

$\hat{\omega}\left(\lambda\right) = [G^T G + \lambda E]^{-1}G^T\psi^{\mathrm{obs}}(2.16)$

The singular value decomposition (SVD) method is used$G = \sum_{i=1} u\Lambda v^T, = min(N, M)$and redefine$\hat{\omega}\left(\lambda\right)$:

$\hat{\omega}\left(\lambda\right) = \frac{\Lambda_i}{\Lambda_i^2 + \lambda}u_i^T v_i\psi^{\mathrm{obs}}(2.17)$

Where Λ is a singular diagonal matrix, Λ_i denotes a singular value component on the diagonal of the matrix and $uv^T$is a singular vector. In terms of calculation efficiency, the equation after SVD can better reflect the information of the main components, which effectively reduces the amount of calculation. Besides, the selection of the regularization parameter λ is also crucial. This paper uses the L-curve method (logarithmic-logarithmic intersection graph ofϕ_d and ϕ_m) to define the optimal value of the regularization parameter (Hansen, 1998).

2.3 Permeability Estimation

Regarding the description of Vogt et al. (2014) in the article, two types of potential field equations are connected by Darcy's velocity formula:

$\sigma\nabla^2\psi = -\rho\gamma Q_V\left(K\right)K\nabla^2\mathrm{h}$ (2.18)

Among them, the spatial change of the pressure p(Pa)denotes the change of the hydraulic head p=ργ∇h. When estimating the permeability K, it is set as an ideal pressure distribution in a uniform half-space. Different pressure distributions can also be applied to the terrain surface or the stratum according to the specific conditions.

$\frac{\sigma\nabla^2\psi}{\nabla^2 h} = -\frac{\rho\gamma}{}$

english$\mu Q_V\left(K\right)K = -\sigma c\left(K\right)$(2.19)

c(k) denotes the sedimentary coupling coefficient on permeability, which is related to the ratio of potential and pressure and is equal to$\frac{\psi}{h}$, μ is the viscosity of the underground medium. Considering the dependence of $Q_V\left(K\right)$ on permeability, we can know:

$\log_{10}\sigma c\left(K\right)\mu = -9.2 + 0.18\log_{10}K$ (2.20)

Combining the above equations, a coupling coefficient value that depends on $K^{0.18}$ can be obtained. Although the permeability dependencies of the coupling coefficient reported in the literature are not as strong as in K1 (Jardani & Revil,2009), Vogt et al. (2014) apply it for study to see maximal effects resulting from permeability dependent coupling. The main workflow of SP inversion is in Figure.1.

Figure 1: Flowchart of the SP inversion and permeability estimation.

3 Groundwater Flow Monitoring Experiment

We select the appropriate experimental measurement area for artificial pumping to achieve the dynamic change of groundwater flow for a long time. The experiment site is in the hydrological observation site of Jilin University (Figure 2). The ERT survey line is 59 m with electrode space is 1m. There are four shallow wells (C6, Ch2, C1, Ch1), and the pumping test is conducted at the well Ch2.

Figure 2. Photos of the survey area, showing the distribution of the ERT survey lines and the water well locations.

3.1 Groundwater Table Hydrological Monitoring

A continuous pumping process is about 12 hours at Well Ch2. After stopping pumping, the groundwater level recovers to the normal within the next 12 hours. Figure 3 visualizes the groundwater level depth in the C6, Ch2, C1, and Ch1 wells around the line. The initial groundwater level is about 2.5m at 3:30 pm. As pumping water, the depth of the groundwater level in Ch2 continuous declines and reaches a peak value (6.5m) around 4:50 am (10 hours later). Then, we stop pump water, and the groundwater level slowly returns to initial depth by groundwater recharge. Both the water level of C6 and Ch1 is little change. The water level in the C1 well has a significant difference after stopping pump water. It indicates that the pumping process only affects the local region around Ch2 and recharges groundwater main from the C1.

Figure 3. Groundwater level monitoring results in the well.

3.2 ERT Monitoring Test

Resistivity tomography is with the Swedish RES2DINV software (Loke, 2006). Figure 4 shows the background resistivity result and source current density inverted by SP data before the pumping test. The first low-resistivity layer is about 0~2.5m, which is surface permeability clay. The current source density at the same depth also shows high values. The current source density, to some extent, reflects the high flow value in the shallow low-resistance area. It is the natural characteristic of low-resistivity soil. Below 2.5m, it is an unsaturated sand layer. The low resistivity zone in the middle part indicates that the groundwater distribution in the shallow well.

Figure 4. a) Background ERT results in the experimental area; b) distribution of underground source current density obtained by SP data inversion.

The time-lapse ERT surveys are more than 20 hours, and delayed resistivity data were collected every 1 hour. The collected data is pre-processed and inverted by RES2DINV software to obtain the resistivity tomography profile in Figure 5 (left). The time-lapse resistivity results have good consistency, which indicates that the raw data has stable quality. Figure 5 (right) is the time-lapse resistivity variation, which is obtained by calculating the difference of time-lapse ERT result. It shows significant spatial and temporal resistivity changes in the pumping area. With the pumping process, the low-resistivity zone gradually becomes deeper. It indicates that the groundwater level declines. Similarly, after pumping is stopped, the water level steadily recovered, and the low-resistivity at the bottom of the formation increased.

Figure 6 shows the results of resistivity changes over time for well Ch2 and C1 at different depths. The resistivity changes around the two wells are similar to the hypothetical formation structure. We believe that there are two types of groundwater recharge zones underground, which have played a key role in different models. In the pumping process, the water level in the CH2 well dominates, and the recharge zone is about 3m to 6 m. However, the recharge range of well C1 is only 3 m to 4 m, and the resistivity change is consistent with the water level record. In the recovery process, the supply area of well Ch2 is below 6 m, showing a trend of low to high, while the supply range of well C1 is below 4 m, showing a continuous increase in resistivity changes.

Figure 5. 2D time-lapse ERT tomography results (left) and resistivity variation in a different time (right).

Figure 6.The resistivity curves around Ch2 and C1

3.3 SP Signal Monitoring

The self-potential signal in the pumping test depends on the movement of the groundwater flow. We also collected the time-lapse SP data in the ERT survey line, and the time interval is 1 hour.

3.3.1 Synthetic Model SP Test

To test the SP signal in the pumping process, we first build a synthetic model according to the pumping experiment (Figure 7). The model (50m $\times$ 15m) has three layers of soil structure, and two drill pipes are set up to simulate the pumping and recovery process. The permeability and conductivity parameters of the model are in Table 1.

Table 1. Distribution of material parameters for numerical simulation

A fluid pressure of 1,000 KPa is applied on the surface. Regarding the electrical boundary conditions, given Neumann conditions at the surface ensures that potential anomalies can be responded to at the surface. Considering that the bottom permeability of the model is extremely low, and the left and right boundaries are far from the channel, the Dirichlet conditions are given to simulate zero at infinity. The potential underground anomaly obtained through the forward modeling problem is shown in figure 8 (up) and figure 9a. The SP amplitude response has significant change at different times. It demonstrates that the rise of groundwater has positive self-potential anomalies, while the abnormal negative signals caused by drawdown. The amplitude of the SP signal decreases with distance from the injection well, which roughly matches the prediction of radial flow in a homogeneous medium around an infinite source.

Regarding the inversion problem, the SP signal is used to retrieve the current source density js. A regularization smoothing term is added to the calculation process to solve the ill-posedness of the potential problem. Where calculate the potential field of the js term (Cardarelli, 2019), we added the conductivity model used in the forward modeling as a constraint term to invert the potential underground distribution (Figure 9b) and the surface SP signal (Figure 8(bottom)). Comparing the anomalous distributions obtained from the two sets of problems, both can adequately characterize the potential response during the decline and rise of the water level, and the results obtained by the inversion of the water level in the bottom part show instability.

Figure 7. Numerical pumping test with a three-layer soil model

Figure 8. The forward SP data (up) and the inverted SP data (bottom)

Figure 9. (a) The forward potential field of groundwater level changes and (b) the inverted potential field

3.3 Time-lapse SP Signal in the Pumping Experiment

Surface time-lapse SP measurements during a pumping test in the ERT survey line and the time interval is 1 hour (Figure 10a), which shows significant SP signal variation during the groundwater flow. The change of real SP data is in agreement with the conclusion of the above SP synthetic model test. The SP field shows local negative anomalies during pumping, which is the result of groundwater level decline in the well. When stopping pumping, the potential anomaly dropped significantly, showing multiple positive anomalies, indicating that the water flow in the bottom replenishment zone penetrated upwards until the pumping equilibrium.

Used the resistivity as a constraint, we estimate the permeability distribution in the test area according to the SP data (Figure 10b, Ikardet al., 2018). Similarly, the electrical boundary conditions we choose are consistent with those of the forward simulation, and the ground boundary is the Neumann boundary condition. The estimated value of permeability information is a scalar quantity, which represents the information state of groundwater flow sensitivity and distribution in the formation. It can be observed that the characteristics of groundwater flow are evident in the two model phases (pumping and recovery), and they are mainly distributed in the shallow formations around Ch2.

Figure 10. (a) Time-lapse SP field in the pumping water experiment,(b) estimated permeability distribution result by SP and ERT coupling coefficient.

4 Discussion

The ERT and SP results show reliable evidence to describe the groundwater pumping and recharge experiments. In Figure11a, we compare the time-lapse hydrological groundwater level monitoring at well Ch2 to the geophysics result. In Figure 11a, the groundwater level increases from the initial depth (2.6m) to 6 m at the pumping water stage (from 3:30 pm to 6:50 am). Then, the groundwater level returns to the initial depth by the groundwater recharge. In the time-lapse ERT results (Figure 11b), because the soil moisture content reduces in the pumping stage, the resistivity increase to the maximum value. Then, it decreases to normal value after the groundwater recharge. It is consistent with the groundwater level change in Figure 11a. There is a positive correlation between the groundwater level and the resistivity.

The SP field at the same depth near the wellhead (Figure 11c) has a negative correlation with the groundwater level change. The estimated permeability by SP and ERT coupling coefficient is in Figure 11d. The primary relationship between the permeability and moisture content in unsaturated soil is that the high moisture content corresponds to low permeability (Gómez et al., 2019; Miao et al., 2018). The reason is that increase in water level depth means that the moisture content reduces. Then, the soil porosity will increase the growth of permeability.

The permeability response is not directional, but it shows a derivative change in the water level detection results. The peak point of the two states during the pumping period is about 7 pm. The permeability value shows a significant increase with the rapid decline of the water level, and the permeability gradually decreases in the saturated state in the late pumping period. In the same way, within the pumping stops, the rise of the groundwater level causes the formation of permeability to increase. When the water level returns to its original state, the permeability is flat with the background value.

Figure 11: a) Time-lapse groundwater level at Well Ch2, b) the resistivity variation around Well Ch2, c) the measured SP signal around Well Ch2, and d) is the estimated permeability by SP and ERT coupling coefficient.

Figure 12: Interpretative scheme of mutual recharge of groundwater flow at pumping and recharge processes.

Based on the following discussion, we build the conceptual model to display the groundwater flow characteristics around well CH2 and well C1 (Figure 12). The process of groundwater flow can be divided into two stages (Figure 12a: pumping and Figure 12b: recovery), and the main layered recharge is concentrated in the changing area of water level. Obviously, in the pumping model, the central formation becomes the main recharge area in the well, and in the recovery stage, the deep formation supplies to the well. The continuous recharge zone around well C1, which corresponds to the low resistivity zone. It can be interpreted as an area of high permeability and high moisture content, both of which provide groundwater recharge.

5 Conclusions

In this paper, we combine the time-lapse ERT and SP data to monitor the groundwater flow variation. Groundwater flow infiltrates and transfers between soil particles and pores, and the moisture content affects the formation to some extent and other parameters. ERT result establishes linkages between the resistivity and moisture content to reveal the change of groundwater flow. Besides, the SP field is sensitive to the change of groundwater flow by groundwater dynamics. The rise and drawdown of groundwater will produce positive and negative SP field, respectively. The pumping water experiment results demonstrate that joint ERT and SP method can provide a reliable result to describe the variation of groundwater flow and understand the qualitative relationship between groundwater flow and its geophysical response.

Data Availability Statement

Data associated with this research are available and can be obtained by contacting the corresponding author.

Acknowledgements

This work are supported by the Natural Science Foundation of China (41874134), the Jilin Excellent Youth Fund (20190103142JH) and the China Postdoctoral Science Foundation 2015M571366

REFERENCES

Carey, A.M., Paige, G.B., Carr, B.J., Dogan, M. (2017). Forward modeling to investigate inversion artifacts resulting from time-lapse electrical resistivity tomography during rainfall simulations. Journal of Applied Geophysical, 145, 39–49.

Darnet, M., Maineult A., and Marquis G. (2004). On the origins of self-potential (SP) anomalies induced by water injections into geothermal reservoirs. Geophysical Research Letters, 31 (19), L19609, doi:10.1029/2004GL020922.

Elédn, L. (1977). Algorithms for regularization of ill-conditioned least squares problems. BIT Numerical Mathematics, 17(2), 134–145.

Gómez Etzar, Broman Viktor, Dahlin Torleif, Barmen Gerhard, Rosberg Jan-Erik. (2019). Quantitative estimations of aquifer properties from resistivity in the Bolivian highlands.H2Open Journal, 2 (1): 113–124. doi:https://doi.org/10.2166/h2oj.2019.007

Hansen, P.C. (1998). Rank-Deficient and Discrete Ill-Posed Problems: Numerical Aspects of Linear Inversion. SIAM, Philadelphia p. 247.

Ikard, S. J., Teeple, A. P., Payne, J. D., et al. (2018). New Insights on Scale-dependent Surface and Groundwater Exchange from a Floating Self-potential Dipole. Journal of Environmental & Engineering Geophysics, 23(2), 261-287. doi: https://doi.org/10.2113/JEEG23.2.261

Jardani, A., Revil, A., Barrash, W., Crespy, A., Rizzo, E., Straface, S., Cardiff, M., Malama, B., Miller, C., Johnson, T. (2009). Reconstruction of the water table from self-potential data: a Bayesian approach. Groundwater, 47, 213–227.

Jardani, A., Revil, A., Bolève, A., Dupont, J.P., Barrash, W, Malama, B. (2007). Tomography of groundwater flow from self-potential (SP) data. Geophysical Research Letters, 34, L24403, doi: http://dx.doi.org/10.1029/2007GL031907.

Jongmans, D., Garambois, S. (2007). Geophysical investigation of landslides: a review. Bulletin De La Société Géologique De France, 178, 101–112.

Li, Y., Oldenburg, D.W. (1998). 3-D inversion of gravity data. Geophysics, 63(1), 109–119.

Linde, N., Revil, A., Bolève, A., Dagès, C., Castermant, J., Suski, B., Voltz, M. (2007). Estimation of the water table throughout a catchment using self-potential and piezometric data in a Bayesian framework. Journal of Hydrology, 334(1-2): 88-89. doi:*https://doi.org/10.1016/*j.jhydrol.2006.09.027.

Loke, M.H. (2006). RES2DINV Rapid 2-D resistivity and IP inversion using the least-squares method. Geotomo Software, Malaysia.

Menke, W. (1984). Geophysical Data Analysis: Discrete Inverse Theory. Academic Press, p. 289.

Minsley, B. J. (2007). Modeling and Inversion of Self Potential Data. Massachusetts Institute of Technology. Doi: http://dspace.mit.edu/handle/1721.1/40863

Niesner, E. (2010). Subsurface resistivity changes and triggering influences detected by continuous geoelectric monitoring. The Leading Edge, 29(8), 952-955.

Ogilvy, R. D., Meldrum, P. I., Kuras, O., Wilkinson, P. B., Chambers, J. E., & Sen, M., et al.(2009). Automated monitoring of coastal aquifers with electrical resistivity tomography. Near Surface Geophysics, 7(6), 367-376.

Oliveti, I., Cardarelli, E. (2019). Self-Potential Data Inversion for Environmental and Hydrogeological Investigations. Pure and Applied Geophysics, 176, 3607–3628. doi: https://doi.org/10.1007/s00024-019-02155-x

Revil, A., Mendonça, C.A., Atekwana, E.A., Kulessa, B., Hubbard, S.S., Bohlen, K.J. (2010). Understanding biogeobatteries: Where geophysics meets microbiology. Journal of Geophysical Research, Biogeosciences, 115, G00G02. Doi: 10.1029/2009jg001065.

Revil, A., Linde, N., Cerepi, A., Jougnot, D., et al. (2007). Electrokinetic coupling in unsaturated porous media. Journal of colloid & interface science, 313, 315–327.

Sill, W.R. (1983) Self-potential modelling from primary flows. Geophysics, 48, 76–86.

Soueid Ahmed, A., Jardani, A., Revil, A., Dupont, J.P. (2013). SP2DINV: A 2D forward and inverse code for streaming potential problems. Computers and Geosciences, 59, 9-16. Doi: https://doi.org/10.1016/j.cageo.2013.05.008.

Trujillo-Barreto, N.J., Aubert-Vásquez, E., Valdès-Sosa, P.A. (2004). Bayesian model averaging in EEG-MEG imaging. NeuroImage, 21(4), 1300–1319.

Vogt, C., Klitzsch, N., Rath, V. (2014). On self-potential data for estimating permeability in enhanced geothermal systems.Geothermics, 51, 201-213.

Tesfaldet, Y. T., AvirutPuttiwongrak. (2019). Seasonal Groundwater Recharge Characterization Using Time-Lapse Electrical Resistivity Tomography in the Thepkasattri Watershed on Phuket Island. Hydrology, 6(2), 36.

Yanan Miao, Xiangfang Li, Yunjian Zhou, Keliu Wu, Yucui Chang, Zhihua Xiao, Nan Wu, Wenji Lin. (2018). A dynamic predictive permeability model in coal reservoirs: Effects of shrinkage behaviour caused by water desorption. Journal of Petroleum Science and Engineering, 168, 533-541. Doi: https://doi.org/10.1016/j.petrol.2018.05.028

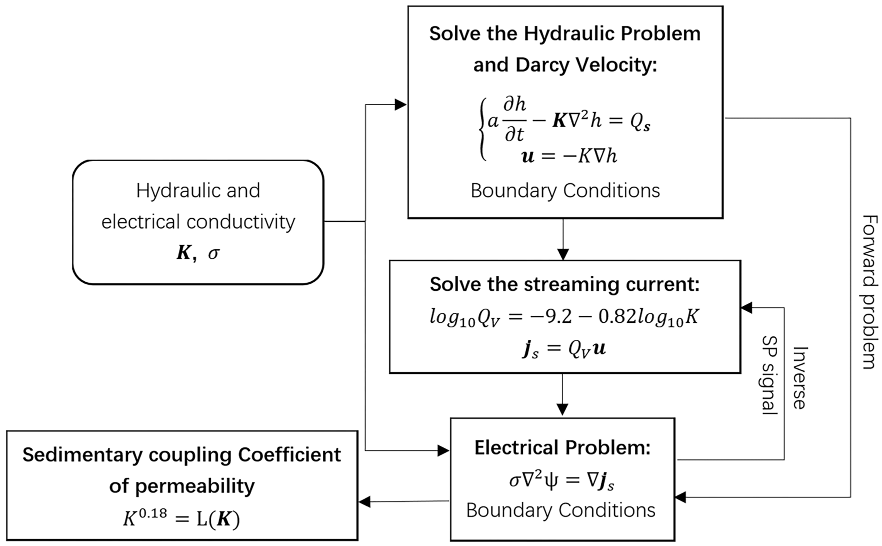

Solve the Hydraulic Problem and Darcy Velocity:
$a\frac{\partial h}{\partial t} - \boldsymbol{K}\nabla^2 h = Q_s$
$\boldsymbol{u} = -K\nabla h$
Boundary Conditions
Hydraulic and electrical conductivity
$\boldsymbol{K}$, σ
Solve the streaming current:
$log_{10}Q_V = -9.2 - 0.82log_{10}K$
$\boldsymbol{j}_s = Q_V\boldsymbol{u}$
Electrical Problem:
$\sigma\nabla^2\psi = \nabla\boldsymbol{j}_s$
Boundary Conditions
Sedimentary coupling Coefficient of permeability
$K^{0.18} = \mathrm{L}(\boldsymbol{K})$
Forward problem
Inverse
SP signal

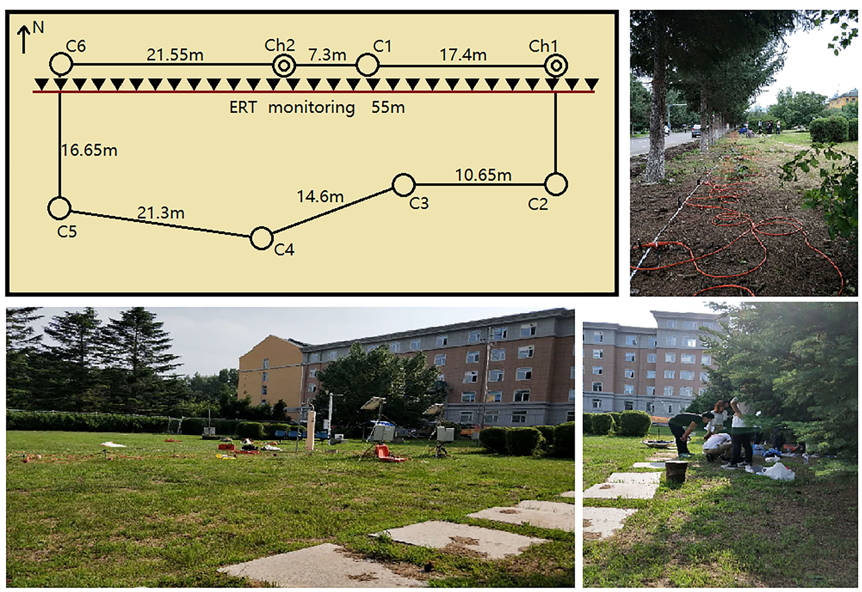

N
C6
21.55m
Ch2
7.3m
C1
17.4m
Ch1
ERT monitoring 55m
16.65m
10.65m
14.6m
C3
C2
C5
21.3m
C4

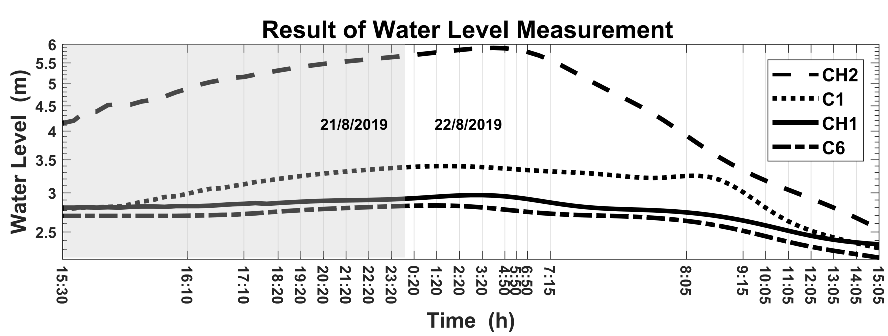

Result of Water Level Measurement
Water Level (m)
Time (h)
21/8/2019
22/8/2019
CH2
C1
CH1
C6
6
5.5
5
4.5
4
3.5
3
2.5
15:30
16:10
17:10
18:20
19:20
20:20
21:20
22:20
23:20
0:20
1:20
2:20
3:20
4:50
5:50
6:50
7:15
8:05
9:15
10:05
11:05
12:05
13:05
14:05
15:05

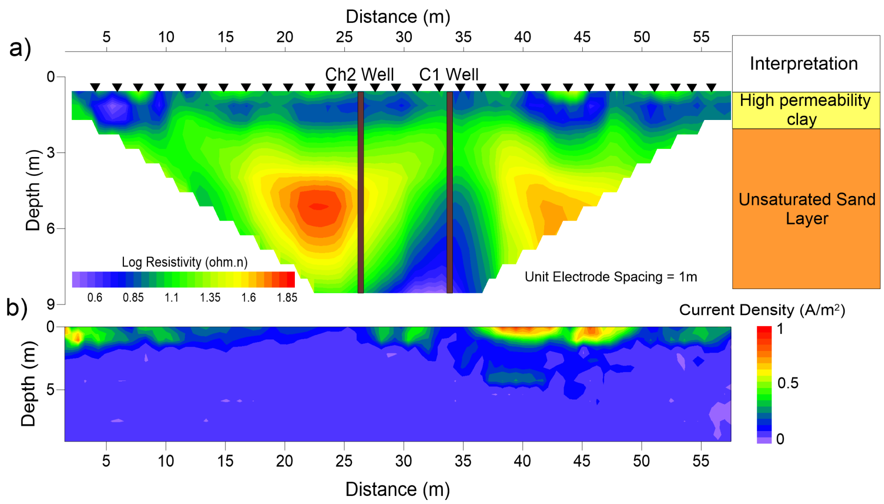
a)
Distance (m)
Ch2 Well
C1 Well
Depth (m)
Log Resistivity (ohm.n)
0.6 0.85 1.1 1.35 1.6 1.85
Unit Electrode Spacing = 1m
Interpretation
High permeability clay
Unsaturated Sand Layer
b)
Current Density (A/m²)
Depth (m)
Distance (m)

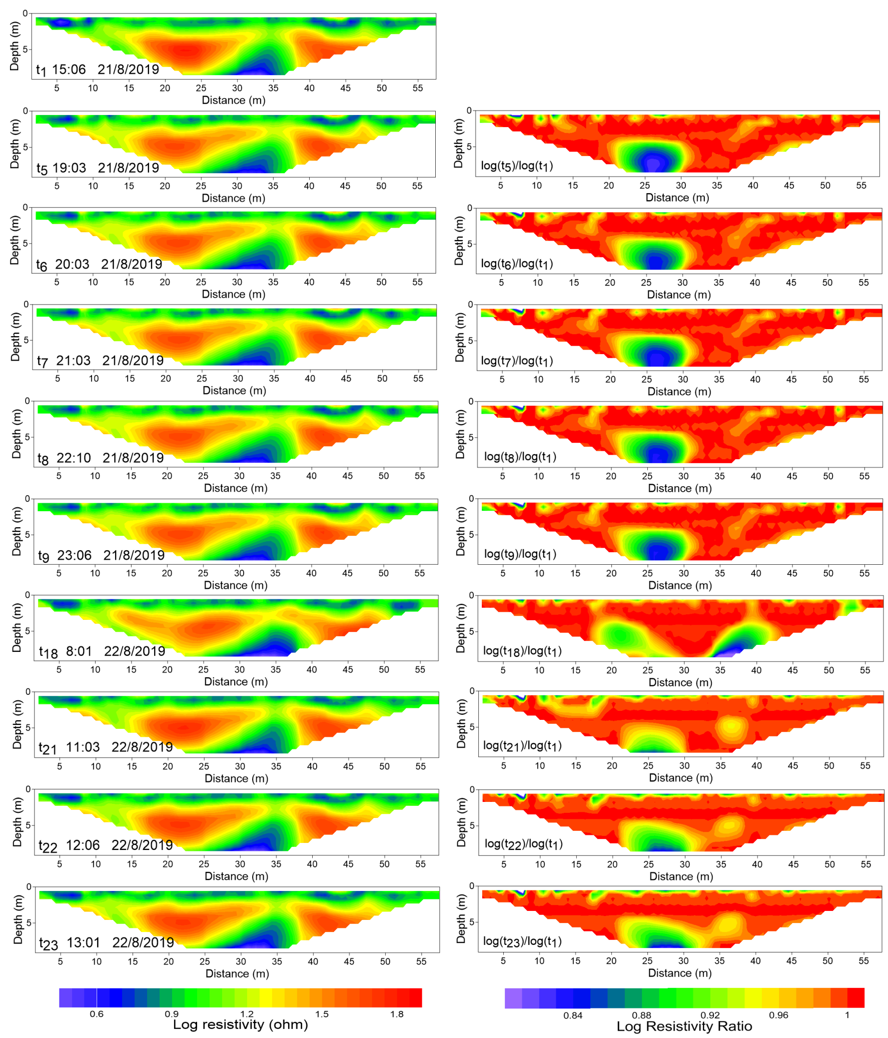
t1 15:06 21/8/2019
t5 19:03 21/8/2019
t6 20:03 21/8/2019
t7 21:03 21/8/2019
t8 22:10 21/8/2019
t9 23:06 21/8/2019
t18 8:01 22/8/2019
t21 11:03 22/8/2019
t22 12:06 22/8/2019
t23 13:01 22/8/2019
log(t5)/log(t1)
log(t6)/log(t1)
log(t7)/log(t1)
log(t8)/log(t1)
log(t9)/log(t1)
log(t18)/log(t1)
log(t21)/log(t1)
log(t22)/log(t1)
log(t23)/log(t1)
Depth (m)
Distance (m)
Log resistivity (ohm)
Log Resistivity Ratio

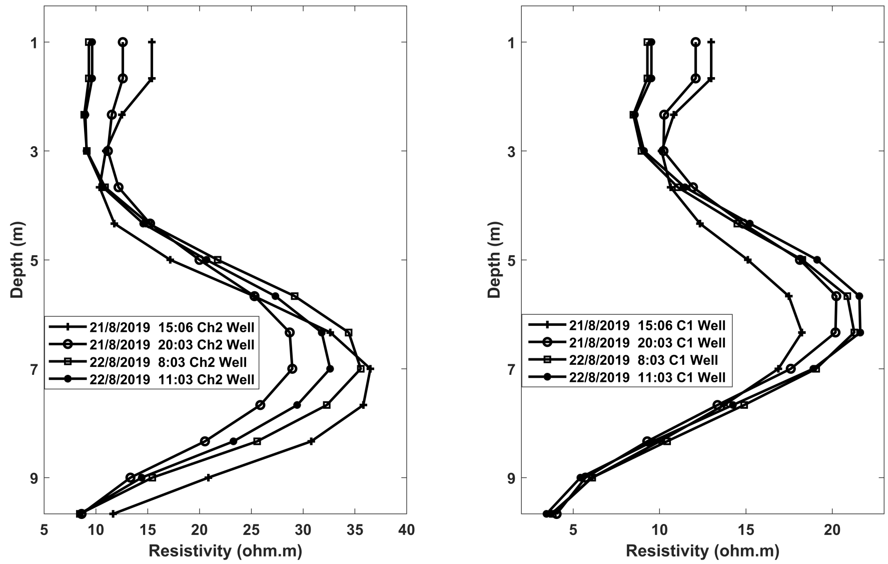

Material	Sandstone	limestone	*granite*	*Permeable conduits*
Conductivity(S/m)	0.0067	0.005	0.0025	0.025
Permeability ($\times10^{-3}$ m^2)	1.0181	1.0176	1.0068	1.0183

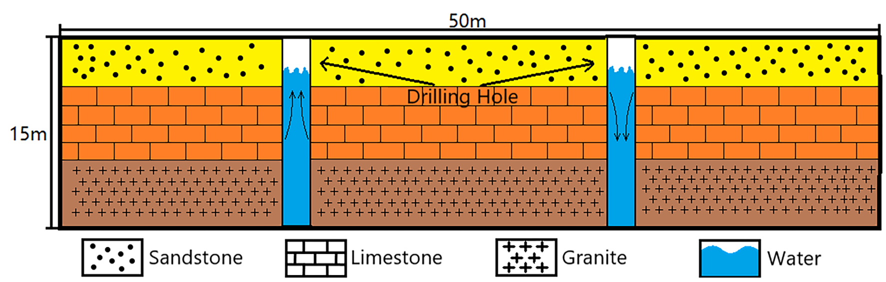

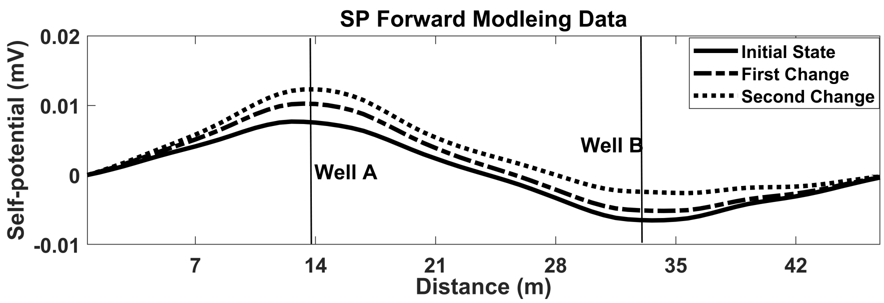
SP Forward Modleing Data
Self-potential (mV)
0.02
0.01
0
-0.01
Initial State
First Change
Second Change
Well A
Well B
7
14
21
28
35
42
Distance (m)

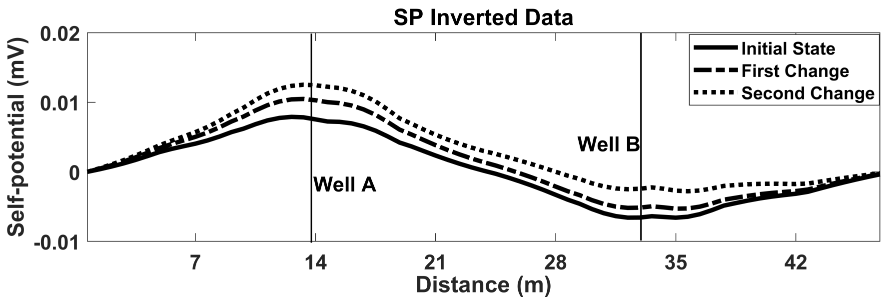
SP Inverted Data
Self-potential (mV)
0.02
0.01
0
-0.01
Initial State
First Change
Second Change
Well A
Well B
7
14
21
28
35
42
Distance (m)

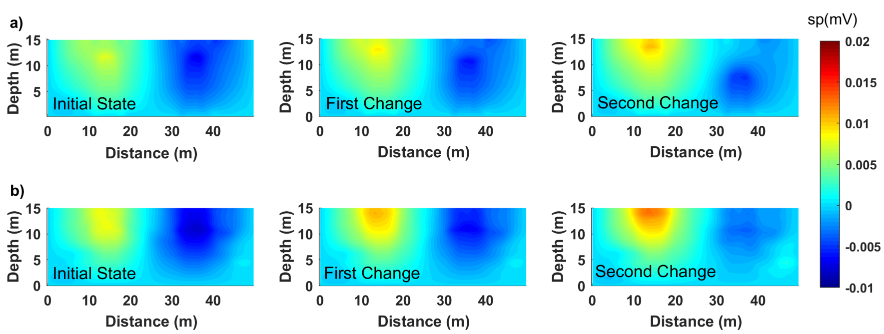
a)
b)
Depth (m)
Distance (m)
Initial State
First Change
Second Change
sp(mV)
0.02
0.015
0.01
0.005
0
-0.005
-0.01

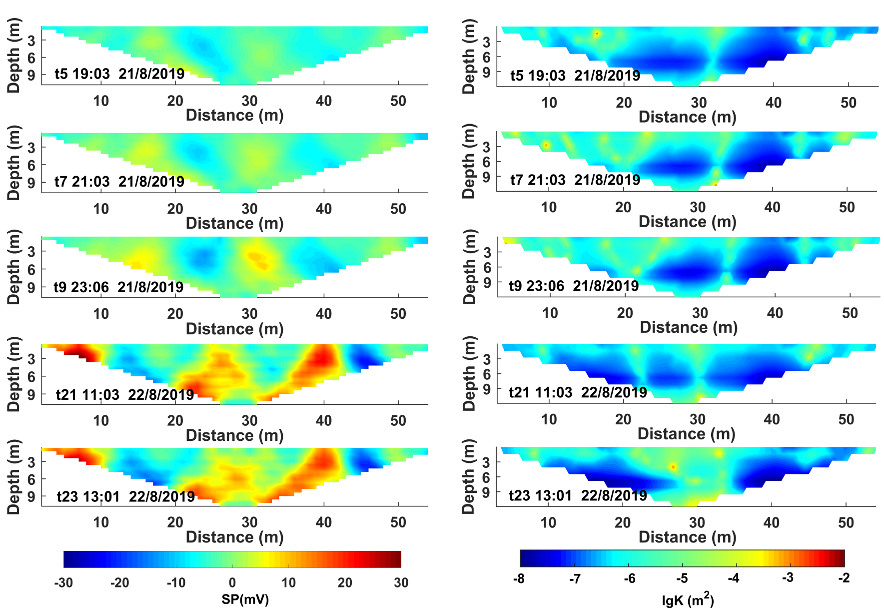
Depth (m)
Distance (m)
t5 19:03 21/8/2019
t7 21:03 21/8/2019
t9 23:06 21/8/2019
t21 11;03 22/8/2019
t23 13:01 22/8/2019
t5 19:03 21/8/2019
t7 21:03 21/8/2019
t9 23:06 21/8/2019
t21 11:03 22/8/2019
t23 13:01 22/8/2019
SP(mV)
lgK (m^2)

figures/figure11/figure11-eps-converted-to.pdf figures/figure12/figure12-eps-converted-to.pdf